Non-Cross Diffusion for Semantic Consistency

Ziyang Zheng* Ruiyuan Gao* Qiang Xu
The Chinese University of Hong Kong
{zyzheng23,rygao,qxu}@cse.cuhk.edu.hk

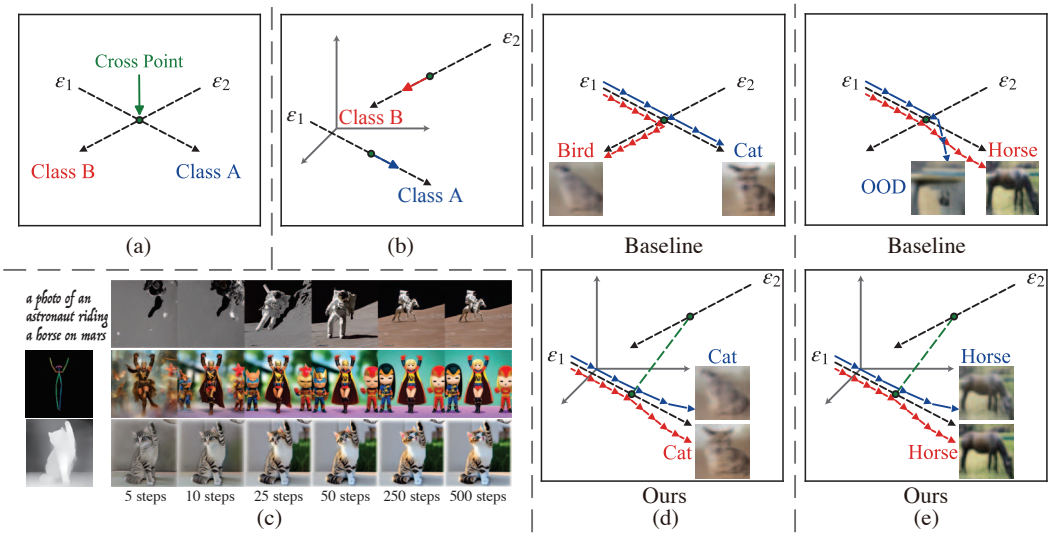

Figure 1. Illustrating XFLOW in Diffusion Models. (a) Demonstrates the ambiguity in training targets caused by crossing flows, leading to the XFLOW problem. (b) Shows how our method eliminates flow crossing by increasing the dimensionality of network inputs, thus resolving the XFLOW problem. (c) Depicts how XFLOW leads to variable sampling results across different steps, undermining deterministic sampling even for Stable Diffusion [20]. (d) *Top*: Highlights the discrepancies between outcomes from reduced steps sampling (blue) versus standard results (from 1000 steps in red) due to XFLOW. *Bottom*: Our method ensures consistent outputs across different sampling steps. (e) *Top*: Exhibits instances where XFLOW causes Out-Of-Distribution (OOD) outcomes in reduced steps sampling (blue) compared to standard results (from 1000 steps in red). *Bottom*: Our approach minimizes the occurrence of OOD samples.

Abstract

In diffusion models, deviations from a straight generative flow are a common issue, resulting in semantic inconsistencies and suboptimal generations. To address this challenge, we introduce 'Non-Cross Diffusion', an innovative approach in generative modeling for learning ordinary differential equation (ODE) models. Our methodology strategically incorporates an ascending dimension of input to effectively connect points sampled from two distributions with uncrossed paths. This design is pivotal in ensuring enhanced semantic consistency throughout the inference process, which is especially critical for applications reliant on consistent generative flows, including various distillation methods and deterministic sampling, which are fundamental in image editing and interpolation tasks.

Our empirical results demonstrate the effectiveness of Non-Cross Diffusion, showing a substantial improvements in semantic consistencies at various inference steps and enhancing the overall performance of diffusion models.

1. Introduction

Diffusion models, as delineated in recent studies [4, 10, 18, 20, 23–25], have exhibited remarkable capabilities in image synthesis, bolstering numerous applications such as text-to-image generation [17, 21], image editing [1, 2, 17, 26], and image inpainting [1, 19]. A key characteristic of these models is their multi-step generative process, which not only allows for correction of the diffusion path [25] but also enhances controllability [5, 7].

Despite these advancements, the inference process in diffusion models typically involves a specific flow, whereas the

*Equal contribution.

training process entails random step selections from multiple flows. This randomness often results in a given training step correlating with diverse flows, creating ambiguity in target identification from the network's perspective, as depicted in Fig. 1(a). We term this phenomenon 'xFLOW'.

xFLOW's emergence during training can hinder the model's optimization at certain steps, leading to a spectrum of generative issues. Notably, it challenges the model's ability to generate samples via a straight flow, compromising deterministic sampling across varying step counts, as shown in Fig. 1(c). It also complicates predicting later sampling steps from earlier ones, limiting the effectiveness of reward models [30] and guided models [4]. Moreover, in the context of distillation, which typically adopts a progressive approach, xFLOW can introduce misleading signals, as evidenced in Rectified Flow [15]. Perhaps most critically, xFLOW can lead to the generation of Out-Of-Distribution (OOD) samples or low-quality samples, especially as sampling step size increases, as illustrated in Fig. 1(d-e).

In this paper, we propose a novel training strategy aimed at resolving the xFLOW challenge in diffusion models. Our method centers on augmenting the input dimensionality to these models, a change that effectively prevents flow crossing. As depicted in Fig. 1(a), the issue at hand arises when two flows intersect, creating ambiguity; the input to the network (for instance, a noisy image) remains constant, yet it is associated with multiple potential targets (such as distinct noises originating from different images). To address this, our approach entails predicting the flow itself during the training phase, as shown in Fig. 1(b). Notably, we utilize the noise predicted by the network as the flow's endpoint, incorporating this element into the model's input. This technique sidesteps the pitfall of using groundtruth noise as input, which would otherwise result in trivial training solutions devoid of substantive learning. For practical implementation, we found ControlNet [31] particularly effective in this context. Additionally, our methodology integrates a bootstrap approach reminiscent of Analog bits [3], which significantly enhances our model's optimization and effectively narrows the gap between training and inference phases."

To evaluate our approach, we introduce the Inference Flow Consistency (IFC) metric, reflecting xFLOW severity. We also utilize Inception Score (IS) [22] and Fréchet Inception Distance (FID) [9] for assessing generation quality. Our models, trained from scratch and compared against baselines on CIFAR-10 [13], demonstrate not only an avoidance of xFLOW but also an enhancement in generation quality. The contributions of this paper include:

- We identify a widespread phenomenon in diffusion models, termed xFLOW, leading to non-straight flow during inference stage that may generate OOD or suboptimal samples.
- We attribute xFLOW's origins to the instability of the target during the training process. Accordingly, we introduce the *Non-Cross Diffusion*, a novel training and inference pipeline to mitigate the xFLOW problem by enhancing input dimensionality.
- Our experiments on both a toy model and the CIFAR-10 dataset demonstrate that our method not only improves the proposed IFC metric by addressing xFLOW, but also significantly enhances other image evaluation metrics, such as IS and FID.

2. Related work

2.1. Diffusion models

Diffusion models, as generative models, learn the reverse denoising process from Gaussian noise to image distribution, achieved through either Markov [10] or non-Markov operations [23]. They are favored over other generative models like GAN [8] and VAE [27] due to their training stability and superior generation quality. Subsequent enhancements to these models primarily concern varied network architectures [12], noise schedulers or losses [18], transition from image space diffusion to latent space [20], and improved sampling techniques [16], with little attention to the xFLOW during training. Rectified Flow [15] noted the mismatch in sampling across different inference steps, a significant distillation issue, but did not analyze it further. Instead, they proposed a workaround using a 2-rectified flow to fit another model to a non-crossing flow between source and target distributions, which depends on a well-trained diffusion model and requires additional retraining. Our paper is the first to examine xFLOW in diffusion and offer solutions.

2.2. Conditional Image Generation

Conditioning techniques are instrumental in managing generated content [6, 20, 28, 29]. For diffusion models, score-based model [25] proposes classifier guidance, which is an efficient method to balance controllability and fidelity using the gradients from a classifier, while classifier-free guidance [11], being another important conditioning technique to diffusion models, trains both conditional and unconditional diffusion models, and combining their score to achieve better controllability. ControlNet [31] employs pretrained encoding layers from billions of images as a backbone to learn diverse conditional controls, which is an architecture adopted in this paper. Analog Bits [3] introduces a technique that conditions the model on its own previously generated samples during iterative sampling, akin to our work. However, Analog Bits mainly aims to enhance sample quality by reusing the previous target, while our focus is to introduce a condition as an extra dimension in the training flow to prevent crossing issues.

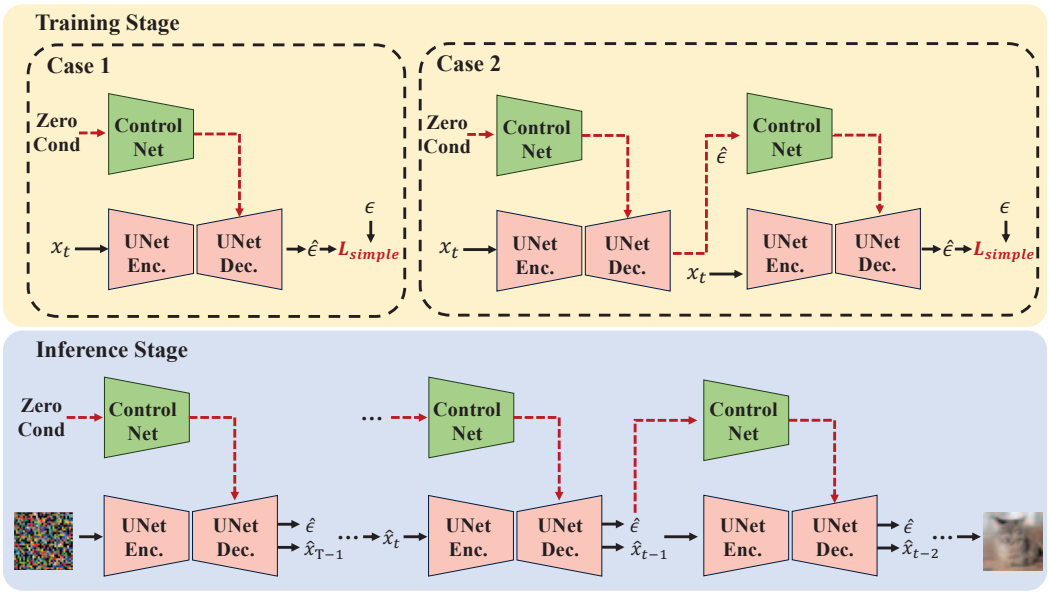

Figure 2. The overview of non-cross diffusion. **Training stage**: The training phase involves two cases. In Case 1, we utilize **0** as the condition and calculate loss function L_{simple} as defined in Eq. 5. For Case 2, we first compute $\hat{\epsilon}$ using **0** as condition. Subsequently, $\hat{\epsilon}$ is employed as the condition to calculate L_{simple}. Throughout the training process, Case 1 is applied with a fixed probability p; otherwise, Case 2 is implemented. **Inference stage**: During the inference phase, **0** is used as the condition in the initial denoising step. This is followed by iterative utilization of the estimated noise from the previous step as the condition for subsequent steps.

3. Method

In this section, we start with a brief review of the formulation of DDPM [10]. Next, we show the drawback of baseline flow and analyze the cause of XFLOW. Then, we introduce *Non-Cross Diffusion* to avoid crossing by ascending dimension of input, together with training, inference, and network architecture of *Non-Cross Diffusion*. Finally, we introduce IFC for evaluating the semantic consistency of the inference flow.

3.1. Preliminary

Given samples from data distribution $x_0 \sim q(x_0)$, DDPM [10] defines a forward noising process q, producing latent variables $x_1, \dots, x_T$ by gradually adding Gaussian noise with a variance schedule $\beta_t \in (0, 1)$ as follows:

$$q(x_1, \dots, x_T) \coloneqq \prod_{t=1}^{T} q(x_t|x_{t-1}), \tag{1}$$

$$q(x_t|x_{t-1}) \coloneqq \mathcal{N}(x_t; \sqrt{1-\beta_t}x_{t-1}, \beta_t\mathbf{I}). \tag{2}$$

With $\alpha_t \coloneqq 1 - \beta_t$ and $\bar{\alpha}_t \coloneqq \prod_{s=0}^{t} \alpha_s$, the marginal $q(x_t|x_0)$ can be derived through Eq. 2 as follows:

$$q(x_t|x_0) = \mathcal{N}(x_t, \sqrt{\bar{\alpha}_t}x_0, (1-\bar{\alpha}_t)\mathbf{I}), \tag{3}$$

$$x_t = \sqrt{\bar{\alpha}_t}x_0 + \sqrt{1-\bar{\alpha}_t}\epsilon, \tag{4}$$

where $\epsilon \sim \mathcal{N}(\mathbf{0}, \mathbf{I})$. Using Bayes theorem, we can calculate the posterior $q(x_{t-1}|x_t, x_0)$ in terms of β_t, α_t and $\bar{\alpha}_t$. There are many different ways to parameterize p_θ to approximate the posterior, while DDPM [10] chooses $p_\theta(x_{t-1}|x_t) = \mathcal{N}(x_{t-1}; \boldsymbol{\mu}_\theta(x_t, t), \sigma_t^2\mathbf{I})$, and propose that predicting ϵ works best with a loss function:

$$L_{simple} = E_{t,x_0,\epsilon}[\|\epsilon - \epsilon_\theta(x_t, t)\|^2], \tag{5}$$

where $\boldsymbol{\mu}_\theta(x_t, t) = \frac{1}{\sqrt{\alpha_t}}(x_t - \frac{\beta_t}{\sqrt{1-\bar{\alpha}_t}}\epsilon_\theta(x_t, t))$

3.2. Understanding Drawbacks of DDPM Flow

Training stage. Given source distribution π_0 (*i.e.*, $q(x_0)$) and target distribution π_1 (*i.e.*, $\mathcal{N}(\mathbf{0}, \mathbf{I})$), we sample two data pairs $(x_0, x_T), (y_0, y_T) \sim \pi_0 \times \pi_1$. During the training stage, assume these two training flows cross at time step t (*i.e.*, $x_t = y_t$). Following Eq. 4, we have:

$$x_t = \sqrt{\bar{\alpha}_t}x_0 + \sqrt{1-\bar{\alpha}_t}\epsilon_x, \tag{6}$$

$$y_t = \sqrt{\bar{\alpha}_t}y_0 + \sqrt{1-\bar{\alpha}_t}\epsilon_y. \tag{7}$$

At the crossing point, both flows aim to minimize the loss function as follows during training:

$$L_{simple} = E_{t,x_0,\epsilon}[\|\epsilon - \epsilon_\theta(x_t, t)\|^2], \tag{8}$$

For given $(x_0, x_T), (y_0, y_T)$ and cross point t, the loss can be reformulated as follows:

$$L_1 = \frac{1}{2}\|\epsilon_x - \epsilon_\theta(x_t, t)\|^2 + \frac{1}{2}\|\epsilon_y - \epsilon_\theta(y_t, t)\|^2, \tag{9}$$

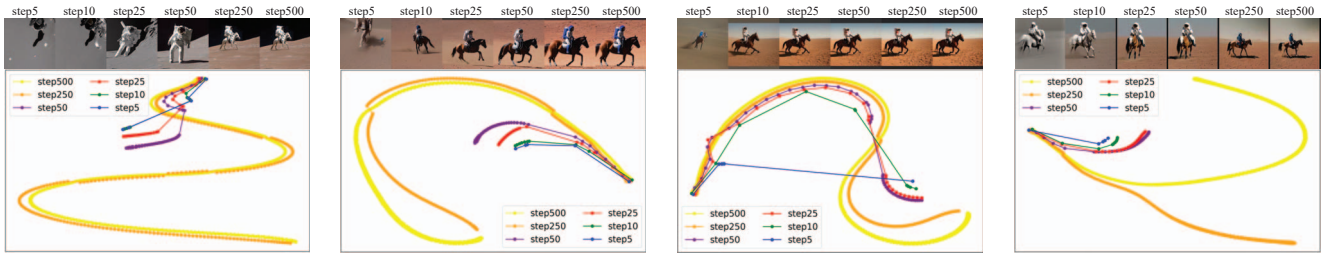

(a) (b) (c) (d)

Figure 3. Generated images and inference flows of Stable Diffusion 1.5 using DDIM scheduler with prompt *"a photo of an astronaut riding a horse on mars"* and negative prompt *"bad, deformed, ugly, bad anotomy"*. (a)-(d) are generated with seed 0,1,2,3 respectively. The results demonstrate that the inference flows across different steps could be quite different at specific time t, which implies the influence of the XFLOW.

where $\epsilon_x = x_T$ and $\epsilon_y = y_T$. To check how the crossing point affects the optimization process, we simplify the target in the formulation of an optimization problem. Since $\epsilon_\theta(x_t, t) = \epsilon_\theta(y_t, t) = \epsilon_\theta(z_t, t)$, we use the notion of ϵ_θ to represent them all.

$$\theta^* = \arg\min_\theta \frac{1}{2}\|\epsilon_x - \epsilon_\theta\|^2 + \frac{1}{2}\|\epsilon_y - \epsilon_\theta\|^2 \tag{10}$$

$$= \arg\min_\theta \frac{1}{2}(\epsilon_x^2 - 2\epsilon_x\epsilon_\theta + \epsilon_\theta^2 + \epsilon_y^2 - 2\epsilon_y\epsilon_\theta + \epsilon_\theta^2) \tag{11}$$

$$= \arg\min_\theta \frac{1}{2}(\epsilon_x^2 + \epsilon_y^2) - (\epsilon_x + \epsilon_y)\epsilon_\theta + \epsilon_\theta^2 \tag{12}$$

$$= \arg\min_\theta \frac{1}{4}(\epsilon_x^2 + 2\epsilon_x\epsilon_y + \epsilon_y^2) - (\epsilon_x + \epsilon_y)\epsilon_\theta + \epsilon_\theta^2 \tag{13}$$

$$= \arg\min_\theta \|\frac{\epsilon_x + \epsilon_y}{2} - \epsilon_\theta\|^2 \tag{14}$$

Hence, with the existence of a crossing point, the optimizing target is equivalent to $\frac{\epsilon_x+\epsilon_y}{2}$. However, since $\epsilon_x \sim \mathcal{N}(\mathbf{0}, \mathbf{I})$ and $\epsilon_y \sim \mathcal{N}(\mathbf{0}, \mathbf{I})$, we have $\frac{\epsilon_x+\epsilon_y}{2} \sim \mathcal{N}(\mathbf{0}, \frac{\sqrt{2}}{2}\mathbf{I})$, which no longer follows standard normal distribution. This implies that at the crossing point, the model is given *an incorrect target*, which will lead to *ambiguity* in data generation (*i.e.*, the denoising process).

Inference stage. Considering the *ambiguity* exists in a trained model, XFLOW, where the generation flow may deviate from the correct direction, results in various failure cases, as illustrated in Fig. 1. We further visualize the inference flow of text-to-image Stable Diffusion in different steps. We save the intermediate latent of each step and visualize the inference flow by using T-SNE. As illustrated in Fig. 3, the visualization demonstrates that Stable Diffusion also shows various inference flows across different steps, which implies the influence of XFLOW. The results in Fig. 3 demonstrate that the XFLOW phenomenon occurs frequently within stable diffusion, which results in sub-optimal or even OOD synthesis.

Besides, we propose that the consequences of XFLOW also depend on the timestep of inference. Specifically, more inference steps, correlating with smaller strides, subtly affect inference flow because the deviation is also smaller and subsequent steps can correct minor errors. On the contrary, fewer inference steps, leading to larger strides, significantly impact the inference flow due to the crossing point, potentially generating inconsistent or OOD samples. Such phenomena will decrease the determinism of diffusion models.

3.3. Non-Cross Diffusion

As analyzed in Sec. 3.2, XFLOW is caused by incorrect training targets. To solve XFLOW, we introduce a new formulation of diffusion models that can avoid crossing points during training, namely *Non-Cross Diffusion*.

Given the fact that latent variables are linear combinations of x_0 and ϵ as in Eq. 4. We can think of the issue with geometry, where training flows are line segments in 2D coordinates, as shown in Fig. 1 (a), with the crossing point as the intersection of two segments. From a basic geometrical concept, *i.e.*, any two distinct lines in a plane can intersect at most once, as long as we can avoid the intersection once, the two segments will never intersect again. Therefore, we aim to eliminate crossing points between any two different training flows, thereby maintaining the integrity and distinctiveness for all of them.

To operationalize this concept, we propose to ascend the dimension of model input. The primary issue with Eq. 9 is that $\epsilon_\theta(x_t, t) = \epsilon_\theta(y_t, t)$ when $x_t = y_t$. To rectify this, we can introduce condition $c^x \neq c^y$ to ensure $\epsilon_\theta(x_t, c^x, t) \neq \epsilon_\theta(y_t, c^y, t)$ and prevent the training flow from crossing. The challenge is identifying $c^x \neq c^y$ given a cross point t and training flow. To solve this, we use x_i, y_i as conditions for each non-crossing step i on the training flow, i.e., $c^x = x_i$ and $c^y = y_i$. Specifically, given $x_t = y_t$, by sampling another point on the flow (*i.e.*, x_i and y_i), we have $x_i \neq y_i$, and thus $[x_i, x_t] \neq [y_i, y_t], \forall i \in [0, T] \setminus \{t\}$. This reminds us that any other samples (x_i) from the same

flow can be used for ascending dimensions. This strategy effectively creates a multidimensional space where the likelihood of training flows intersecting is significantly reduced.

Selection of Condition. x_i is effective for ascending dimensions only if it is significantly different from x_t. Given the continuity of both linear combination and diffusion models, we propose to ascend the dimension with either initial noise x_T (*i.e.*, ϵ) or the data point x_0. Furthermore, we find the distance between randomly sampled noise is stable while the distance between data points may not. Take image data as an example, for two randomly sampled noise $n_1, n_2 \in \mathbb{R}^{H\times W\times C}$, we have $E[\|n_1 - n_2\|^2] = 2CHW$. Besides, we can only get the initial noise during the inference stage. Therefore, using the initial noise x_T for dimension ascending is more practical.

3.4. Inference Flow Consistency

To better evaluate the consistency of the inference flow for image generation, we propose a metric by computing the similarity between intermediate generated image $\hat{x}_0^t$ in timestep t and the final generated image $\hat{x}_0$ based on peak signal-to-noise ratio (PSNR) as follows:

$$\text{IFC} = \frac{1}{T}\sum_{t=0}^{T} PSNR(\hat{x}_0^t, \hat{x}_0). \tag{15}$$

Training Stage. The cornerstone of our training strategy is to circumvent trivial solutions and avoid training collapse. To achieve this, we replace the use of initial noise ϵ with predicted noise $\hat{\epsilon}$. This substitution is critical in refining our model's predictive accuracy since it can effectively avoid trivial solutions. However, in the initial training phase, the substantial error $\|\epsilon - \hat{\epsilon}\|^2$ indicates $\hat{\epsilon}$'s poor estimation. Hence, a bootstrap strategy is introduced to $\hat{\epsilon}$ during training, preventing misleading estimation of $\hat{\epsilon}$ and thus enhancing learning robustness in the early stage.

As illustrated in Fig. 2, our training objective is formulated as follows:

$$\min_\theta E_{t,x_t,\epsilon,}[\|\epsilon - \epsilon_\theta(x_t, \hat{\epsilon}_t, t)\|^2], \tag{16}$$

where $x_t = \sqrt{\bar{\alpha}_t}x_0 + \sqrt{1-\bar{\alpha}_t}\epsilon$. During training, we apply the bootstrap as follows: 1) with a fixed probability p, we set $\hat{\epsilon}_t = \mathbf{0}$ (*i.e.*, Case 1 in Fig. 2); 2) at other cases, $\hat{\epsilon}_t$ is assigned the value of $\epsilon_\theta(x_t, \mathbf{0}, t)$ (*i.e.*, Case 2 in Fig. 2). We do not back-propagate through estimated noise $\hat{\epsilon}_t$.

Inference Stage. As illustrated in Fig. 2, during the inference stage, to alleviate the computational costs, we use estimated noise in the previous step instead of the current step as the condition and iteratively predict $\hat{\epsilon}$ as follows:

$$\hat{\epsilon}_T = \epsilon_\theta(\hat{x}_T, \mathbf{0}, T), \tag{17}$$

$$\hat{\epsilon}_t = \epsilon_\theta(\hat{x}_t, \hat{\epsilon}_{t+1}, t), t < T. \tag{18}$$

When the number of inference steps is large, the discrepancy between $\hat{\epsilon}_t$ and $\hat{\epsilon}_{t+1}$ is small, which ensures the performance of our method.

Network Architecture. Inspired by ControlNet [31], to efficiently use $\hat{\epsilon}_t$, *Non-Cross Diffusion* employs an additive U-net branch, with $\hat{\epsilon}_t$ as input. For optimization, modifications are introduced, specifically removing all zero convolution layers and initializing the addictive encoder for $\hat{\epsilon}_t$ with the original U-net. The output is incorporated into the U-net decoder via addition. The whole network is trained end-to-end from scratch.

A change in training flow direction at a specific timestep yields notable differences in pre- and post-change images, reducing PSNR. This can be effectively assessed for consistency across inference stages using our PSNR-based metric.

4. Experiment

In this section, we discuss our experimental results on toy examples (Sec. 4.1) and image generation tasks (Sec. 4.2), as well as ablation studies (Sec. 4.3) and further discussion for *Non-Cross Diffusion* (Sec. 4.4).

4.1. Toy Examples

In this section, we follow the setting in Rectified Flow [15], drawing a training dataset from Gaussian mixture $\pi_0 \times \pi_1$. Given a sample $\{x_0^i, x_1^i\}$ from $(X_0, X_1) \sim \pi_0 \times \pi_1$, for baseline model, we train a 3-layer MLP $v_\theta(z, t)$ to transfer from π_0 to π_1 with l2-loss as follow:

$$\min_\theta \|v_\theta(x_t^i, t) - (x_1^i - x_0^i)\|_2,$$
$$x_t^i = tx_1^i + (1-t)x_0^i, t \in [0, 1).$$

Our method enhances this approach by incorporating an additional dimension with the estimated target as follows:

$$\min_\theta \|v_\theta([x_t^i, \hat{c}_t^i], t) - (x_1^i - x_0^i)\|_2,$$
$$\hat{c}_t^i = \begin{cases} \mathbf{0} & \text{p}\leq 0.5 \\ v_\theta([x_t^i, \mathbf{0}], t) & \text{otherwise} \end{cases}$$

with $p \sim U(0, 1)$. The inference process is also similar to our proposed method, *i.e.*, we use the estimated target in the previous step as the condition.

Results. As shown in Fig. 4, the baseline model's inference flow alters direction at the intersection of two flows due to an erroneous loss function (Eq. 14), generating OOD samples. For toy examples, by adding an extra dimension using the estimated result, our method prevents flow intersection, maintaining consistent inference flow direction and effectively inhibiting OOD sample generation.

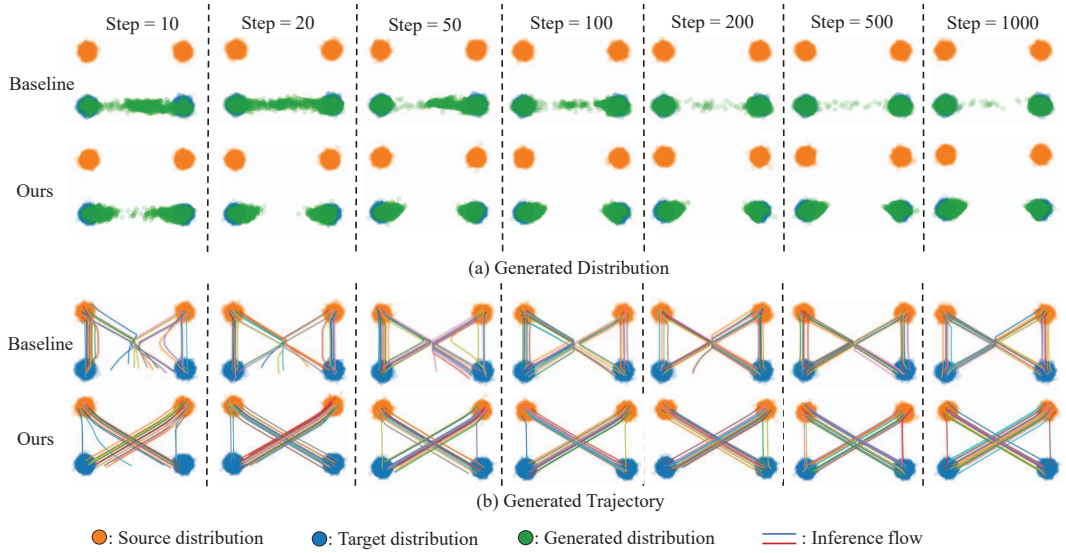

Figure 4. Results of the Toy Model. (a) Comparison of Generated Distributions: This panel illustrates the distributions generated by the baseline model and our proposed model. As the number of inference steps decreases, the baseline model tends to produce a significant number of out-of-distribution (OOD) samples. In contrast, our model effectively mitigates the generation of OOD samples. (b) Trajectory Analysis: This panel compares the generated trajectories of the baseline and our models. The baseline model's inference flow often redirects at the intersection point, leading to a target OOD distribution as the inference steps decrease. Our method, however, maintains a consistent direction in the inference model, thereby straightening the trajectory.

	DDIM-1000		DDIM-100		DDIM-50		DDIM-20		DDIM-10		DDIM-5	
Method	IS	FID	IS	FID	IS	FID	IS	FID	IS	FID	IS	FID
iDDPM	9.02	4.70	8.99	5.65	8.89	6.61	8.59	9.82	8.20	15.91	7.09	31.37
iDDPM‡	9.10	4.82	8.93	5.75	8.79	6.71	8.65	9.89	8.14	16.06	7.08	31.21
Ours	**9.51**	**2.88**	**9.22**	**3.93**	**9.10**	**5.31**	8.77	9.87	7.97	20.63	6.20	50.25
Ours†	9.34	3.40	9.15	4.21	9.05	5.08	**8.84**	**7.75**	**8.50**	**12.85**	**7.45**	**27.83**

Table 1. We compare the performance of baseline and our method. We generate 50k samples using DDIM with inference steps in {1000, 100, 50, 20, 10, 5}. ‡We expand the U-net encoder to ensure the same model size as ours. †We use an inference strategy similar to the training stage. Specifically, we first give **0** as condition and get estimated noise $\hat{\epsilon}_t$, then we take $\hat{\epsilon}_t$ as condition and compute denoised image $\hat{x}_{t-1}$.

4.2. Experiments on Image Generation

Implementation Details. Our models are trained on CIFAR-10 [13] and MNIST [14], with MNIST images resized to 32×32. The fidelity of generated samples is evaluated using IS [22] and FID [9] and inference flow consistency with IFC. As a baseline, we train iDDPM [18] from scratch with the same UNet. Training for CIFAR-10 follows iDDPM except using L_{simple} only and with 250k steps. For MNIST, training is similar to CIFAR-10 but with 100k steps. In this paper, we consider unconditional generations on each dataset (*i.e.* w/o class labels).

Comparison of Sampling Quality. Tables 1 and 2 compare our model's performance with a baseline model in generating CIFAR-10 and MNIST images. Fig. 7 visualizes the generated CIFAR-10 images, where our model notably outperforms the baseline, especially at {1000, 100, 50} inference steps. The decreased number of inference steps and increased strides enlarge the discrepancy in estimated noise between steps, introducing bias and performance decline during inference. To counter this, we suggest conditioning on the current step's estimated noise. This augments image quality generated by our method even at smaller steps in {20, 10, 5}. Besides, our model outperforms the baseline on MNIST at steps {1000, 100, 50}. The adapted sampling strategy also enhances our model's performance on MNIST as the number of inference steps decreases.

DDIM-1000		DDIM-100		DDIM-50	
Method	FID	Method	FID	Method	FID
iDDPM	8.02	iDDPM	8.26	iDDPM	9.12
Ours	**7.13**	Ours	**7.72**	Ours	9.06
Ours†	7.52	Ours†	7.91	Ours†	**8.76**

Table 2. We compare the performance of baseline and our method on MNIST. We generate 50k samples using DDIM with inference steps in {1000, 100, 50}. †We use an inference strategy similar to the training stage.

(a) Baseline (b) Ours

Figure 5. Here are the generated images using DDIM with inference steps in {5, 10, 25, 50, 100, 200, 500, 1000} on CIFAR-10. For baseline method, the semantic information of image with small inference step and large inference step could be greatly different, which implies that the inference flow changes its direction at some timesteps.

(a) Baseline (b) Ours

Figure 6. Here are the generated images using DDIM with inference steps in {5, 10, 25, 50, 100, 200, 500, 1000} on MNIST.

	IFC					
DDIM Step	1000	100	50	20	10	5
iDDPM	**28.58**	29.72	30.85	33.94	39.51	46.11
Ours	28.37	**29.96**	**31.4**	**35.11**	**40.21**	**47.96**

Table 3. We compare the consistency of baseline and our method on CIFAR-10. We generate 1000 samples using DDIM with inference steps in {1000, 100, 50, 20, 10, 5}.

Comparison of Inference Consistency. Table 3 reveals our method's superior consistency over the baseline on CIFAR-10 at inference steps {50, 20, 10, 5}, in terms of IFC, achieved by preventing XFLOW. The impact of XFLOW is minimal for larger steps ({1000, 100}), resulting in similar IFC between our method and the baseline. Fig. 5 and Fig. 6 illustrate the visualization results of generated images under different steps on CIFAR-10 and MNIST. The results further demonstrate higher consistency compared with baselines, indicating a straighter inference flow.

4.3. Ablation Study

In this section, we verify the effectiveness of each component through ablation studies.

	Setting	IS	FID
Bootstrap	w/o bootstrap	5.93	79.70
	exp-schedule	9.22	5.24
	fix-prob (Ours)	**9.38**	**4.84**
Condition	$\hat{x}_0$ condition	**9.64**	20.21
	mid. condition	7.15	59.09
	$\hat{\epsilon}$ condition (Ours)	9.38	**4.84**
Network	Double Unet	**9.65**	6.26
	ControlNet-based (Ours)	9.38	**4.84**
Inference strategy	zero condition	9.06	6.43
	ϵ condition	7.86	27.00
	$\hat{\epsilon}$ condition (Ours)	**9.38**	**4.84**

Table 4. Ablation study. We generate 10k samples using DDIM with 1000 inference step.

Ablation of bootstrap. Table 4 demonstrates the impact of the bootstrap strategy. We experimented with three settings: without bootstrap (w/o bootstrap, where $\hat{\epsilon}_t = \epsilon_\theta(x_t, \mathbf{0}, t)$ is consistently applied), exponential schedule (exp-schedule, where the probability p increases exponentially), and fixed probability (fix-probability, where $p = 0.5$). The findings reveal that lacking a bootstrap strategy can notably degrade model performance.

Ablation of condition. We scrutinize the impact of varying conditions on our method. The $\hat{x}_0$ condition implies the model utilizes the predicted image as the condition, while the mid. condition uses the midpoint of training flow (*i.e.* $\frac{\hat{x}_0+\hat{\epsilon}}{2}$). During inference, each technique employs its corresponding condition. As in Table 4, mid. performs suboptimally, presumably due to proximity to the training flows' intersection, as mentioned in Sec. 3.3. Benefiting from its stability, $\hat{\epsilon}$ as a condition leads to a significant FID improvement over $\hat{x}_0$ condition.

Ablation of architecture. We also examine a Double U-net variant, *i.e.*, doubling U-net's input channel to accommodate $\hat{\epsilon}$ input. As Table 4 shows, the ControlNet-based model

(a) Baseline (b) Ours

Figure 7. Displayed are the generated images of baseline model and our model using DDIM with inference step of 1000 on CIFAR-10. The results demonstrate our model's superior image generation capabilities, significantly reducing the occurrence of OOD samples.

enhances FID by 1.42, likely because the two inputs serve distinct roles, and the additive branch enables effective differentiation between them, thereby facilitating training.

Ablation of inference strategy. We also consider several inference strategies applied after training (we utilize a trained $\hat{\epsilon}$-conditioned model). These inference strategies include the Zero condition (utilizing $\mathbf{0}$), the ϵ condition (using initial noise ϵ), and the $\hat{\epsilon}$ condition (employing estimated noise $\hat{\epsilon}$). Performance significantly deteriorates under the ϵ condition due to ϵ-$\hat{\epsilon}$ discrepancy. Though our model circumvents training ambiguity, the Zero condition marginally compromises performance during inference due to potential redirection at cross points in the inference flow.

4.4. Discussion

This section offers an alternative perspective to understand our *Non-Cross Diffusion*. The inclusion of $\hat{\epsilon}_t$ in the model input is seen as a strong conditional constraint, which we propose can reduce the variability of semantic information, thus lessening the severity of XFLOW during inference.

Specifically, the $\hat{\epsilon}_t$ condition in *Non-Cross Diffusion* is highly specific at the pixel level, making it an exceptionally stringent constraint. Consequently, *Non-Cross Diffusion* effectively mitigates the XFLOW issue. An interesting question arises: how would XFLOW be influenced by other forms of conditions with varying degrees of strength? To investigate this, we employed the pre-trained ControlNet model for empirical analysis and results.

Fig. 1(c) shows text conditional images from Stable Diffusion [20], as well as pose conditional and depth conditional images from ControlNet [31]. The text condition images at steps {5, 10, 25, 50, 250, 500} present a significant shift in the semantic content of the images at each step. In contrast, pose conditional images demonstrate more consistent semantic content across steps: the pose of superhero remains the same but the background and the style still show a large variation. The depth conditional images keep the highest consistency across different steps, despite some variability in details such as the background and the pattern. Therefore, we hypothesize that stronger conditions ease the severity of XFLOW.

5. Conclusion

In this study, we have addressed the XFLOW phenomenon in diffusion models, characterized by deviations in generative flow that result in semantic inconsistencies and suboptimal image generation. Our novel approach, '*Non-Cross Diffusion*', innovates in the realm of generative modeling by adopting ordinary differential equation models. Our empirical investigations, including both a toy example and the CIFAR-10 image dataset, demonstrate the substantial efficacy of the *Non-Cross Diffusion* approach. The results show a marked reduction in semantic inconsistencies at various inference stages and significant improvements in the overall performance of diffusion models.

Looking Ahead. The identification of XFLOW as a critical issue during inference opens new avenues for research and application optimization. Despite the effectiveness of the proposed *Non-Cross Diffusion* approach on mitigating XFLOW, we acknowledge the challenges associated with retraining large-scale diffusion models such as Stable Diffusion. However, we are optimistic that future research will find ways to integrate these improvements into existing models, potentially circumventing the need for extensive retraining. This paper lays the groundwork for such advancements, aiming to enhance the reliability and quality of diffusion model outputs.

Acknowledgements. This work was supported in part by the CUHK Research Matching Scheme under Grant No. 7106937, 8601130, and 8601440.

References

[1] Omri Avrahami, Dani Lischinski, and Ohad Fried. Blended diffusion for text-driven editing of natural images. In *Proceedings of the IEEE/CVF Conference on Computer Vision and Pattern Recognition (CVPR)*, pages 18208–18218, June 2022. 1

[2] Tim Brooks, Aleksander Holynski, and Alexei A. Efros. Instructpix2pix: Learning to follow image editing instructions. In *Proceedings of the IEEE/CVF Conference on Computer Vision and Pattern Recognition (CVPR)*, pages 18392–18402, June 2023. 1

[3] Ting Chen, Ruixiang Zhang, and Geoffrey Hinton. Analog bits: Generating discrete data using diffusion models with self-conditioning. *arXiv preprint arXiv:2208.04202*, 2022. 2

[4] Prafulla Dhariwal and Alexander Nichol. Diffusion models beat gans on image synthesis. *Advances in neural information processing systems*, 34:8780–8794, 2021. 1, 2

[5] Ying Fan and Kangwook Lee. Optimizing ddpm sampling with shortcut fine-tuning. *arXiv preprint arXiv:2301.13362*, 2023. 1

[6] Ruiyuan Gao, Kai Chen, Enze Xie, Lanqing Hong, Zhenguo Li, Dit-Yan Yeung, and Qiang Xu. Magicdrive: Street view generation with diverse 3d geometry control. *arXiv preprint arXiv:2310.02601*, 2023. 2

[7] Ruiyuan Gao, Chenchen Zhao, Lanqing Hong, and Qiang Xu. Diffguard: Semantic mismatch-guided out-of-distribution detection using pre-trained diffusion models. In *Proceedings of the IEEE/CVF International Conference on Computer Vision*, pages 1579–1589, 2023. 1

[8] Ian Goodfellow, Jean Pouget-Abadie, Mehdi Mirza, Bing Xu, David Warde-Farley, Sherjil Ozair, Aaron Courville, and Yoshua Bengio. Generative adversarial nets. *Advances in neural information processing systems*, 27, 2014. 2

[9] Martin Heusel, Hubert Ramsauer, Thomas Unterthiner, Bernhard Nessler, and Sepp Hochreiter. Gans trained by a two time-scale update rule converge to a local nash equilibrium. *Advances in neural information processing systems*, 30, 2017. 2, 6

[10] Jonathan Ho, Ajay Jain, and Pieter Abbeel. Denoising diffusion probabilistic models. *Advances in neural information processing systems*, 33:6840–6851, 2020. 1, 2, 3

[11] Jonathan Ho and Tim Salimans. Classifier-free diffusion guidance. *arXiv preprint arXiv:2207.12598*, 2022. 2

[12] Tero Karras, Miika Aittala, Timo Aila, and Samuli Laine. Elucidating the design space of diffusion-based generative models. *Advances in Neural Information Processing Systems*, 35:26565–26577, 2022. 2

[13] Alex Krizhevsky, Geoffrey Hinton, et al. Learning multiple layers of features from tiny images. *Tech Report*, 2009. 2, 6

[14] Yann LeCun, Léon Bottou, Yoshua Bengio, and Patrick Haffner. Gradient-based learning applied to document recognition. *Proceedings of the IEEE*, 86(11):2278–2324, 1998. 6

[15] Xingchao Liu, Chengyue Gong, and Qiang Liu. Flow straight and fast: Learning to generate and transfer data with rectified flow. *arXiv preprint arXiv:2209.03003*, 2022. 2, 5

[16] Cheng Lu, Yuhao Zhou, Fan Bao, Jianfei Chen, Chongxuan Li, and Jun Zhu. Dpm-solver: A fast ode solver for diffusion probabilistic model sampling in around 10 steps. *Advances in Neural Information Processing Systems*, 35:5775–5787, 2022. 2

[17] Alex Nichol, Prafulla Dhariwal, Aditya Ramesh, Pranav Shyam, Pamela Mishkin, Bob McGrew, Ilya Sutskever, and Mark Chen. Glide: Towards photorealistic image generation and editing with text-guided diffusion models, 2022. 1

[18] Alexander Quinn Nichol and Prafulla Dhariwal. Improved denoising diffusion probabilistic models. In *International Conference on Machine Learning*, pages 8162–8171. PMLR, 2021. 1, 2, 6

[19] Aditya Ramesh, Prafulla Dhariwal, Alex Nichol, Casey Chu, and Mark Chen. Hierarchical text-conditional image generation with clip latents, 2022. 1

[20] Robin Rombach, Andreas Blattmann, Dominik Lorenz, Patrick Esser, and Björn Ommer. High-resolution image synthesis with latent diffusion models. In *Proceedings of the IEEE/CVF conference on computer vision and pattern recognition*, pages 10684–10695, 2022. 1, 2, 8

[21] Chitwan Saharia, William Chan, Saurabh Saxena, Lala Li, Jay Whang, Emily L Denton, Kamyar Ghasemipour, Raphael Gontijo Lopes, Burcu Karagol Ayan, Tim Salimans, Jonathan Ho, David J Fleet, and Mohammad Norouzi. Photorealistic text-to-image diffusion models with deep language understanding. In S. Koyejo, S. Mohamed, A. Agarwal, D. Belgrave, K. Cho, and A. Oh, editors, *Advances in Neural Information Processing Systems*, volume 35, pages 36479–36494. Curran Associates, Inc., 2022. 1

[22] Tim Salimans, Ian Goodfellow, Wojciech Zaremba, Vicki Cheung, Alec Radford, and Xi Chen. Improved techniques for training gans. *Advances in neural information processing systems*, 29, 2016. 2, 6

[23] Jiaming Song, Chenlin Meng, and Stefano Ermon. Denoising diffusion implicit models. *arXiv preprint arXiv:2010.02502*, 2020. 1, 2

[24] Yang Song and Stefano Ermon. Generative modeling by estimating gradients of the data distribution. *Advances in neural information processing systems*, 32, 2019. 1

[25] Yang Song, Jascha Sohl-Dickstein, Diederik P Kingma, Abhishek Kumar, Stefano Ermon, and Ben Poole. Score-based generative modeling through stochastic differential equations. *arXiv preprint arXiv:2011.13456*, 2020. 1, 2

[26] Narek Tumanyan, Michal Geyer, Shai Bagon, and Tali Dekel. Plug-and-play diffusion features for text-driven image-to-image translation. In *Proceedings of the IEEE/CVF Conference on Computer Vision and Pattern Recognition (CVPR)*, pages 1921–1930, June 2023. 1

[27] Arash Vahdat and Jan Kautz. Nvae: A deep hierarchical variational autoencoder. *Advances in neural information processing systems*, 33:19667–19679, 2020. 2

[28] Yijun Yang, Ruiyuan Gao, Yu Li, Qiuxia Lai, and Qiang Xu. What you see is not what the network infers: detecting adversarial examples based on semantic contradiction. *arXiv preprint arXiv:2201.09650*, 2022. 2

[29] Yijun Yang, Ruiyuan Gao, and Qiang Xu. Out-of-distribution detection with semantic mismatch under masking. In *European Conference on Computer Vision*, pages 373–390. Springer, 2022. 2

[30] TaeHo Yoon, Kibeom Myoung, Keon Lee, Jaewoong Cho, Albert No, and Ernest K Ryu. Censored sampling of diffusion models using 3 minutes of human feedback. *arXiv preprint arXiv:2307.02770*, 2023. 2

[31] Lvmin Zhang, Anyi Rao, and Maneesh Agrawala. Adding conditional control to text-to-image diffusion models. In *Proceedings of the IEEE/CVF International Conference on Computer Vision*, pages 3836–3847, 2023. 2, 5, 8